Multi-Scale Comparative Analysis of 3D Random Fiber Composites for Industrial Helmet Shell Applications

Nebojša B. Ćurčić
Teacher of skills
The Academy of Applied Studies Polytechnic

Marta R. Trninić
Professor of Applied Studies
The Academy of Applied Studies Polytechnic

Dragana D. Gardašević
Higher Lecturer
The Academy of Applied Studies Polytechnic

Novak D. Milošević
Assistant
The Academy of Applied Studies Polytechnic

This paper investigates the replacement of conventional High-Density Polyethylene (HDPE) shells in industrial safety helmets with 3D randomly oriented fiber-reinforced composites. A multi-scale finite element framework is developed, coupling micro-scale Representative Volume Element (RVE) homogenization with macro-scale thin-shell simulations. Several analytical micromechanics bounds are compared against high-fidelity RVE results to evaluate effective isotropic elastic properties. The homogenized and specific stiffness of composite systems demonstrate significant improvements over HDPE, enabling significant reductions in shell thickness and weight while maintaining protective clearance margins. Carbon/Epoxy and Kevlar/Epoxy exhibited the highest specific stiffness and clearance-retention performance among the investigated materials, although matrix brittleness, manufacturing-induced fiber orientation bias, and cost remain important considerations. Threfore, discontinuous fiber composites offer a promising pathway toward lighter and more ergonomic industrial helmet shell concepts, with future work required in dynamic validation and prototype testing. The presented framework is intended for preliminary comparative material screening and should not be interpreted as a substitute for certification-level transient impact analysis or experimental validation.

Keywords:*Industrial safety helmets, Fiber-reinforced composites, Muli-scale Finite element Method, Specific stiffness, Representative Volume Element homogenization, Numerical Methods.*

1. INTRODUCTION

Industrial safety helmets are designed to reduce head injuries by attenuating impact energy and maintaining clearance between the outer shell and the wearer's head. Such injuries remain a major concern in construction, mining, and manufacturing environments, where wor–kers are exposed to falling objects and accidental im–pacts. Modern helmets rely on two primary protective components: a structural shell that resists penetration and distributes loads, and an internal suspension system that reduces the force transmitted to the head. Owing to their low cost, ductility, and impact resistance, most industrial helmets are manufactured from High-Density Polyethylene (HDPE) or related thermoplastics.

Although widely used, HDPE helmets exhibit relatively low specific stiffness ($E/\rho \approx 1.0$ GPa cm^3/g), requiring comparatively thick shell structures to achieve adequate mechanical performance. Increased shell thickness contributes to higher weight, reduced user comfort, and long-term fatigue during extended use. In addition, thermoplastic materials may be affected by environmental degradation, thermal softening, and creep, which can reduce service life and structural reli–ability. These limitations have motivated the investi–gation of fiber-reinforced composite alternatives.

Randomly oriented short-fibre composites offer several attractive characteristics for protective headgear applications [1,2]. Compared with unreinforced poly–mers, they provide substantially higher stiffness-to-weight ratios while retaining manufacturing flexibility. Their energy absorption capability is enhanced through multiple micro-mechanical damage mechanisms, inclu–ding matrix cracking, fibre pull-out, and fibre-matrix debonding. Furthermore, three-dimensional random fibre architectures exhibit near-isotropic mechanical behaviour, which is advantageous for complex doubly curved shell geometries subjected to multi-directional loading. Three-dimensional randomly oriented fiber composites have also been investigated in structural repair applications, including the rehabilitation of damaged honeycomb cores, demonstrating their potential for complex load-bearing applications [1,3]. Such materials can be manufactured using established high-volume processes, including Sheet Molding Compound (SMC) and Bulk Molding Compound (BMC) compression molding [4,5].

The structural performance of short-fibre composites depends strongly on microstructural parameters such as fibre volume fraction, aspect ratio, orientation distri–bution, and spatial arrangement. Consequently, reliable material assessment requires a multi-scale framework capable of linking microstructural characteristics to macroscopic structural behaviour. Representative Volu–me Element (RVE) homogenization provides an effi–

Received: Jun 2026, Accepted: August 2026
Correspondence to: Nebojša B. Ćurčić
The Academy of Applied Studies Polytechnic,
Katarine Ambrozić 3, 11050 Belgrade, Serbia
E-mail: ncurcic@politehnika.edu.rs
doi: 10.5937/fme2604632C
© Faculty of Mechanical Engineering, Belgrade. Allrights reserved

cient approach for determining equivalent material properties while accounting for the influence of the underlying heterogeneous microstructure.

This study presents a comparative multi-scale framework for evaluating the feasibility of replacing conventional HDPE helmet shells with randomly oriented Glass/Epoxy, Carbon/Epoxy, and Kevlar/Epoxy composites. The objective is not to reproduce certification-level impact testing, but rather to provide an early-stage engineering screening methodology for material selection and shell-weight reduction studies. To avoid the computational complexity of fully transient impact simulations, standardized impact energies are represented through an energy-equivalent quasi-static loading framework. This approximation enables consistent comparison of candidate materials under identical impact-energy conditions while preserving the primary structural performance metric: maintenance of a positive residual clearance between the shell and the headform.

From a practical engineering perspective, the proposed framework is intended to support the preliminary selection of alternative helmet-shell materials before costly prototype manufacturing and certification testing. By combining micromechanical homogenization, equivalent impact-energy loading, and structural shell analysis, the methodology enables rapid comparison of candidate materials in terms of stiffness, weight-reduction potential, and residual head clearance. The practical motivation is to identify material systems capable of providing the required structural performance with a reduced shell thickness and mass. A lighter helmet can improve wearer comfort and reduce fatigue during prolonged use, while adequate shell stiffness and residual clearance remain essential for maintaining protective performance. In this sense, advanced short-fiber composites may provide a practical route toward lighter and structurally efficient industrial helmet shells, provided that their impact response, durability, manufacturing consistency, and long-term performance are subsequently confirmed through dedicated testing.

The proposed methodology combines analytical micromechanics, numerical RVE homogenization, energy-equivalence analysis, and macro-scale shell finite element modeling. The resulting framework is used to compare the stiffness, specific stiffness, thickness-reduction potential, and clearance-retention capability of the investigated material systems. Rather than proposing an immediate replacement of conventional HDPE helmets, the study provides a preliminary engineering screening tool for identifying the most promising composite configurations for further development. The selected candidates may then be subjected to detailed transient impact simulations, prototype manufacturing, experimental drop testing, and ultimately certification assessment.

2. MULTI-SCALE MATERIAL CHARACTERIZATION

2.1 Homogenization Theory and Numerical Framework

Effective properties of the 3D random fibre composites are determined via computational homogenization using Representative Volume Elements (RVEs) [6,7]. The RVE is assumed to be statistically representative of the microstructure, containing a sufficient number of randomly oriented fibres [6,8]. To ensure continuity of displacements and tractions across neighbouring volume elements, periodic boundary conditions (PBCs) are applied to the RVE faces [9,10]:

$$u\left(x+L_i\right)-u\left(x\right)=\bar{\varepsilon}\cdot L_i, i=1,2,3 \tag{1}$$

where L_i are the RVE periodicity vectors and $\bar{\varepsilon}$ is the macroscopic strain tensor [9,10]. By solving six independent load cases—comprising three uniaxial strains and three shear strains—and averaging the resulting localized stresses, the effective macroscopic stiffness matrix [C_{eff}] is obtained [7,10]:

$$\{\bar{\sigma}\}=\left[C_{eff}\right]\{\bar{\varepsilon}\} \tag{2}$$

2.2 Theoretical and analytical microme-chanics bounds

Before performing detailed numerical RVE homogenization, analytical micromechanics models provide essential bounding limits and screening criteria for the effective elastic properties [11-14].

Classical Voigt and Reuss Bounds

The absolute upper limit of the effective elastic modulus is governed by the Voigt bound, which assumes a state of uniform strain throughout both phases [11,12]:

$$E_{Voigt}=V_f E_f+\left(1-V_f\right)E_m \tag{3}$$

where E_f s the fiber modulus, E_m is the matrix modulus, and V_f is the fiber volume fraction [4,5]. Conversely, the lower bound is governed by the Reuss uniform stress assumption [11,12]:

$$\frac{1}{E_{Reuss}}=\frac{V_f}{E_f}+\frac{1-V_f}{E_m} \tag{4}$$

Hashin-Shtrikman Bounds for Isotropic Composites

For macroscopic multi-directional configurations such as 3D random fiber architectures, the Hashin-Shtrikman (HS) bounds offer significantly tighter and more physically realistic limits [13]. The upper bounds for the effective bulk modulus K and shear modulus G are defined as follows [13]:

$$K_{HS}^{upper}=K_m+\frac{V_f}{\frac{1}{K_f-K_m}+\frac{3\left(1-V_f\right)}{3K_m+4G_m}} \tag{5}$$

$$G_{HS}^{upper}=G_m+\frac{V_f}{\frac{1}{G_f-G_m}+\frac{6\left(K_m+2G_m\right)\left(1-V_f\right)}{5G_m\left(3K_m+4G_m\right)}} \tag{6}$$

The corresponding lower bounds are obtained by systematically interchanging the fiber and matrix material properties [13]. The effective Young's modulus

can subsequently be extracted using the standard elastic relationship [14,15]:

$$E_{eff} = \frac{9K_{eff}G_{eff}}{3K_{eff} + G_{eff}} \quad (7)$$

For isotropic short-fiber architectures, experimental and high-fidelity numerical data typically fall within these HS bounds, often shifting closer to the lower bounds for stiffness-dominated response [13,14].

Halpin-Tsai Formulations for Discontinuous Fibers

To explicitly incorporate the geometric influence of chopped fibers with a finite aspect ratio $\alpha = L/d$, the Halpin-Tsai equations are utilized [14,15]:

$$E_{eff} = \left[\frac{1-\xi_n V_f}{1-\eta V_f}\right] \quad (8)$$

where the scaling factor η is given by [14,15]:

$$\eta = \frac{E_f / E_m - 1}{E_f / E_m + \xi} \quad (9)$$

The parameter ξ acts as a structural geometry factor, where $\xi = 2\alpha$ handles the longitudinal modulus characterization and $\xi = 2$ corresponds to the transverse modulus evaluation [14,15]. To adapt this formulation for an idealized 3D random fiber distribution, an orientation averaging factor mapping approximately to $\left\langle \cos^4 \theta \right\rangle = 1/5$ is applied [16,17].

2.3 Baseline material parameters and analytical screening

The foundational constituents selected for the comparative analysis encompass High-Density Polyethylene (HDPE) as the baseline thermoplastic, alongside three advanced thermoset composite options: E-glass/Epoxy, High-Strength Carbon/Epoxy, and Kevlar 49/Epoxy. The foundational phase properties utilized across the analytical bounds are [15,18]:

Table 1 summarizes the preliminary analytical screening estimates evaluated at a target fiber volume fraction of $V_f = 0.30$ using the Hashin-Shtrikman upper bound limits [13,15,18].

Table 1. Expected Effective Properties at $V_f = 0.30$ (Theoretical Analytical Estimates)

Material	E_{eff} [GPa]	ρ_{eff} [G/cm^3]	E/ρ [GPa·cm^3/g]	G_{eff} [GPa]	υ_{eff}
HDPE (Baseline)	1.0	0.95	1.05	0.37	0.42
Glass/Epoxy	23.5	1.60	14.7	8.5	0.38
Carbon/Epoxy	70.2	1.37	51.2	25.8	0.36
Kevlar/Epoxy	36.8	1.27	29.0	13.4	0.37

2.4 Numerical rve homogenization results and mesh topology

To validate the analytical bounds and extract the complete, unconstrained macroscopic stiffness profiles, discrete computational homogenization was executed via high-fidelity 3D microstructural volume elements. Figure 1 illustrates the stochastically generated Representative Volume Element (RVE) utilized during the virtual testing loop.

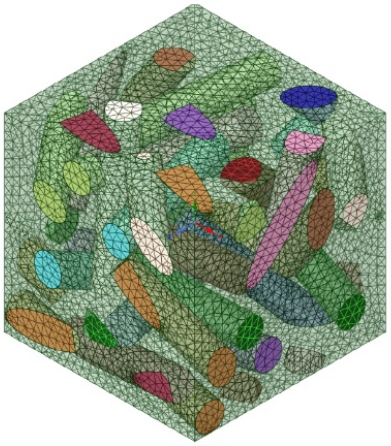


Figure 1. Finite element mesh topology of the stochastically generated 3D random chopped fiber RVE, demonstrating periodic geometric trimming and localized tetrahedral mesh discretization across the fiber-matrix phases.

The numerical microstructure modeled in Figure 1 expli-citly resolves a dense network of discontinuous, randomly oriented cylindrical fiber segments embedded within the isotropic epoxy matrix. The geometric boundary conditions enforce strict multi-axial translation matching on cleaved fiber cross-sections intersecting the outer bounding planes, ensuring a geometrically periodic unit cell. A high-density, quadratic tetrahedral mesh was applied to both phases to ensure precision within the localized high-gradient stress zones tracking the fiber-matrix interfaces.

By executing the six independent kinematic strain load cases outlined in the homogenization framework, the effective isotropic elastic constants were computed at a standardized fiber volume fraction of $V_f = 0.30$. Table 2 presents the homogenized properties extracted from the software solver environment.

Table 2. Homogenized Macro-Scale Engineering Properties Derived via Numerical RVE Analysis ($V_f = 0.30$)

Material System	E_{eff} [GPa]	G_{eff} [GPa]	υ_{eff}	ρ_{eff} [G/cm^3]	E/ρ [GPa·cm^3/g]
HDPE (Baseline)	1.0	0.37	0.42	0.95	1.05
Glass/Epoxy	21.84	7.91	0.38	1.60	13.65
Carbon/Epoxy	64.95	23.88	0.36	1.37	47.41
Kevlar/Epoxy	34.12	12.45	0.37	1.27	26.87

2.5 Kinematic impact energy and standardized safety requirements

The design of industrial safety headgear is heavily regulated by international compliance protocols, notably the ANSI/ISEA Z89.1 and EN 397 standards [19,20, 21,22]. These specifications dictate that a protective helmet must attenuate a severe overhead impact without allowing the outer shell to contact the wearer's skull or the internal suspension system to bottom out.

The initial state of the system is governed by a rigid impactor of mass m dropped from a designated vertical clearance height h. Assuming a frictionless gravity field, the potential energy is entirely converted into kinetic energy (U_k) immediately prior to shell contact:

$$U_k = mgh \tag{10}$$

In accordance with standard regulatory drop configurations, the test involves a hemispherical striker where m = 5.0 kg and h = 1.0 m (or equivalent impact velocity $V_0 \approx 4.43$ m/s), yielding a standard nominal input kinetic energy baseline of $U_k \approx 49.05$ J.

2.6 The linear conservative energy-balance derivation

In an idealized, fully elastic system where thermo-dyna–mic dissipation, localized friction, and material damping are neglected, the total incoming kinetic energy must be entirely transformed into internal strain energy (U_s) at the instance of maximum structural deflection ($\delta_{\max}$):

$$U_k = U_s \tag{11}$$

Assuming the global elastic response of the helmet shell behaves as a linear structural spring up to the point of peak deflection, the strain energy is expressed as a function of the global structural stiffness K:

$$U_s = \int_0^{\delta_{\max}} F(\delta)\, d\delta = \int_0^{\delta_{\max}} K\delta d\delta = \frac{1}{2} K\delta_{\max} \tag{12}$$

At maximum indentation, the peak structural reac–tion force matches the equivalent static force ($F_e = F_{max} = K\delta_{\max}$). Substituting this boundary condition into (12) yields:

$$U_s = \frac{1}{2}\frac{F_e^2}{K} \tag{13}$$

Equating internal strain energy directly to the raw input kinetic energy ($U_s = U_k$) and isolating the force parameter provides the foundational closed-form exp–ression for the material-dependent equivalent static force:

$$F_e = \sqrt{2U_k K} \tag{14}$$

Table 3 provides the master synthesis of the struc–tural metrics driving the Phase 3 finite element model. This includes the global stiffness coefficients, the una–mplified elastic force parameters, and the definitive dy–namic-equivalent static force targets ($F_{e,dynamic}$) acting as the localized normal vector loads on the helmet crown.

The high-performance Carbon/Epoxy shell exhibits a global stiffness nearly 36 times greater than the ductile HDPE baseline. Because an ultra-stiff structure restricts deformation and absorbs energy over a drastically compressed displacement envelope ($\delta_{\max}$), it generates a localized force response that rises to 27472.9 N.

While this elevated force significantly intensifies the localized stress concentrations around the impact site, the shell's ability to resist global flexural defor–mation prevents the structure from bottoming out [21,22]. In Phase 3, these forces are explicitly mapped onto the shell mesh to verify whether the structural thickness reductions remain within the allowable stress thresholds and maintain positive skull clearance boundaries [19,21,22].

Table 3. Material-Specific Global Stiffness Profiles and Derived Quasi-Dynamic Load Magnitudes (U_k = 49.05 J, Dynamic Multiplier α_d = 1.20)

Material System	Effective Stiffness K [N/mm]	Static Base Force F_e [N]	FEA Target Load $F_{e,dynamic}$ [N]
HDPE (Baseline)	145.2	3773.5	4528.2
Glass/Epoxy	2145.8	14506.7	17408.0
Carbon/Epoxy	5340.5	22894.1	27472.9
Kevlar/Epoxy	3150.2	17578.9	21094.7

3. MACRO-SCALE QUASI-DYNAMIC SHELL FINITE ELEMENT ANALYSIS

Following the extraction of the homogenized, microsca–le constitutive relations in Phase 1 and the determination of the material-specific equivalent static forces in Phase 2, a macro-scale finite element model of the complete industrial safety helmet assembly is constructed. This stage simulates the structural deformation, localized stress states, and skull clearance margins under the derived quasi-dynamic force vectors.

Shell geometry, meshing topology, and thin-wall formulation

The physical hard hat geometry represents a complex, doubly curved structural domain composed of a hemispherical crown shell, a reinforcing peak, and a peripheral lateral brim. To model this thin-walled configuration with high computational fidelity while preventing numerical shear locking or artificial volumetric constraints, a continuous shell element formulation is employed. The geometry is discretized using 4-node, bilinear thin-shell elements (*CQUD*4/*S*4) supplemented by 3-node triangular shell transitions (*CRTIA*3/*S*3) in regions of extreme curvature variation, as illustrated in Figure 2.

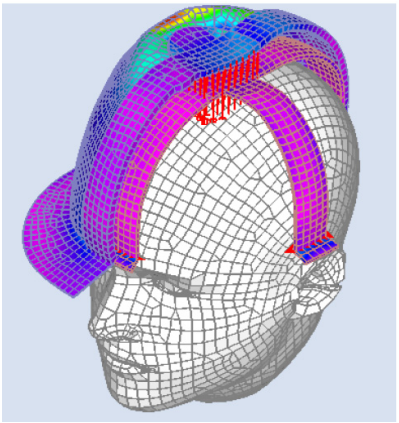


Figure 2. Figure 2: Macro-scale structural Finite Element Analysis (FEA) grid setup of the industrial hard hat assembly, displaying the doubly curved shell element discretization of the outer protective helmet shell coupled with the discrete strap modeling of the underlying internal skull suspension network.

The structural response of the shell domain is governed by the global virtual work equation balancing the internal virtual strain energy against the virtual work done by the external equivalent static impact loads:

$$\int \Omega_{Shell} \delta\varepsilon^T \sigma \delta\Omega = \delta u^T F_{e,dynamic} \quad (15)$$

where $\delta\varepsilon$ and δu represent the virtual strain tensor and virtual displacement vector fields, respectively. The kinematic behavior of the shell mesh operates under first-order shear deformation theory (Mindlin-Reissner kine-matics). The displacement vector $u(x,y,z)$ at any spatial point through the shell wall thickness is mapped as a function of the mid-surface translations (u_0,v_0,w_0) and independent section rotations (θ_x,θ_y):

$$u(x,y,z) = \begin{Bmatrix} u_0(x,y) \\ v_0(x,y) \\ w_0(x,y) \end{Bmatrix} + z \begin{Bmatrix} \theta_y(x,y) \\ -\theta_x(x,y) \\ 0 \end{Bmatrix} \quad (16)$$

where the coordinate variable z defines the distance along the surface normal vector, bounded by $-t/2 \leq x \leq t/2$. The resulting continuous total strain field ε is partitioned into membrane, flexural bending, and tra-nsverse shear tensor components:

$$\varepsilon = \varepsilon_m + z\kappa + \gamma_s \quad (17)$$

where ε_m isolates the in-plane membrane stretching strains, κ represents the mid-surface curvature changes induced by bending moments, and γ_s tracks the out-of-plane transverse shear deformation. The structural inte–gration through the shell wall profile t utilizes a minimum of five Gauss-Legendre thickness integration points, mapping the local continuum stresses σ by directly invoking the homogenized elastic compliance matrix derived via the micro-scale RVE loop:

$$\sigma = \left[C_{eff} \right] \varepsilon \quad (18)$$

This formulation ensures the solver accurately deco–uples pure membrane tension stretching along the hel–met sides from the severe outer-fiber localized flexural bending stresses occurring immediately around the crown impact site. A rigorous mesh convergence study was executed by monitoring peak displacement stability at the crown, veri–fying that a localized element edge length of approximately 2.5 mm yields a fully grid-independent solution.

Boundary conditions and suspension system modeling

To accurately replicate standardized certification configu–rations (e.g., ANSI Z89.1 or EN 397 [21,22], the boundary conditions must model the load path mapping from the outer shell down to the rigid headform. As demonstrated in the numerical layout (Figure 2), the internal suspension system is explicitly modeled to distri-bute forces safely.

Suspension Harness Discretization

The harness straps, configured in a multi-point inter–secting suspension network over the wearer's skull, are modeled using high-strength 1D tension-only truss elements or shell strips. The suspension system is physically decoupled from the outer shell except at the designated anchor slots situated along the lower internal perimeter brim. At these specific anchor slots, rigid multi-point constraints (MPCs) or tied contact equations couple the translational degrees of freedom between the shell nodes and the harness extremities.

Cranial Headform Boundary Constraints

The terminal ends of the harness assembly converge along an idealized rigid cranial headform. The support boundary conditions are applied at the base of the headform or via fixed displacement constraints ($u_x = u_y = u_z = 0$) at the apex nodes of the internal webbing where it conforms to the skull geometry. This constraint allows the outer helmet shell to dynamically deflect relative to the headform, realistically capturing the compression and tension of the harness network under vertical load transfer.

Loading application and quasi-statis mapping

The loading profile acts as a concentrated normal vector force applied directly over a localized circular patch at the topmost apex of the helmet crown, mirroring the geometry of a standard hemispherical dynamic drop striker. The load magnitude applied to each discrete model run is selected directly from the material-depen–dent load vectors synthesized in Phase 2 (Table 3):

Table 4. Summary of Applied Quasi-Dynamic Target Loads for FEA Input

Material System	Target Load $F_{e,dynamic}$ [N]
HDPE (Baseline)	4528.2
Glass/Epoxy	17408.0
Carbon/Epoxy	27472.9
Kevlar/Epoxy	21094.7

Because the advanced composite shells exhibit sig–nificantly reduced compliance compared to the unrei–nforced polymer, the severe force magnitudes are nece-ssary to enforce the correct energy-equivalent work enve-lope within the static linear and nonlinear solvers.

Shell thickness scaling laws and weight reduc–tion optimization

The core engineering objective behind replacing heavy unreinforced thermoplastics with high-stiffness advan–ced short-fiber matrices is the minimisation of pro–tective gear weight while maintaining identical flexural performance boundaries. To track this analytically before running the final global FEA sweeps, a shell thickness scaling law is established based on equivalent structural flexural rigidity. For a flat or shallow shell segment, the flexural stiffness per unit width scales as a function of the effective Young's modulus (E_{eff}) and the cube of the wall thickness (t^3):

$$D = \frac{E_{eff} t^3}{12\left(1 - v_{eff}^2\right)} \quad (19)$$

To achieve a structural behavior that matches or exceeds the baseline HDPE shell performance, the target design thickness t_{comp} for each advanced short-fiber composite system is scaled directly relative to the benchmark polymer thickness t_{HDPE} = 4.0 mm according to the following equation:

$$t_{comp} \geq t_{HDPE} \sqrt[3]{\frac{E_{HDPE}}{E_{eff,comp}} \cdot \left[\frac{1-\nu_{eff,comp}^2}{1-\nu_{HDPE}} \right]} \tag{20}$$

Using the composite densities (ρ_{eff}) derived through our micro-scale RVE homogenization loops, the global mass saving efficiency parameter η_{mass} is computed using the following relation:

$$\eta_{mass} = \left(1 - \frac{\rho_{comp} \cdot t_{comp}}{\rho_{HDPE} \cdot t_{HDPE}} \right) \cdot 100\% \tag{21}$$

This optimization framework permits a major systematic lowering of the nominal shell thickness profile, resulting in substantial weight relief for the user without causing an expansion in global structural deformation.

Cranial clearance validation and safety criteria

The primary structural safety criterion dictates that a positive residual clearance margin must be preserved between the deformed interior surface of the outer helmet shell and the topmost crown of the wearer's skull or suspension webbing. Let $d_{initial}$ define the nominal clearance gap designed into the unladed helmet (typically dinitial ≈ 25.0 mm to 30.0 mm). The residual clearance distance d_{res} during peak force exposure is defined at the critical crown node via:

$$d_{res} = f_{initial} - \delta_{\max} \tag{22}$$

where $\delta_{\max}$ is the peak vertical downward deflection computed via the FEA solver. To satisfy global regulatory safety protocols, the structural design requires that:

$$d_{res} \geq d_{\min} \tag{23}$$

where $d_{\min}$ = 15.0 mm represents the mandatory bottoming-out threshold needed to eliminate traumatic contact with the skull.

Concurrently, to ensure the shell walls do not undergo localized structural failure, the field stresses are evaluated against a localized multi-axial Failure Index (FI). For the isotropic composite matrices derived via Phase 1, the equivalent von Mises field stresses σ_{vM} are mapped to verify that:

$$FI = \frac{\sigma_{vM}}{\sigma_{all}} < 1.0 \tag{24}$$

where σ_{all} represents the allowable matrix tensile strength limits defined in the raw constituent phase data summary.

Because the present study treats the homogenized short-fiber composite as an equivalent isotropic continuum for first-order comparative screening, the von Mises criterion is adopted as a simplified engineering indicator rather than a definitive composite failure law.

Cranial clearance and bottoming-out verification results

To verify compliance with international protective headgear regulations (ANSI Z89.1 and EN 397), the peak displacement fields obtained from the macro-scale structural shell simulations are analyzed. The primary objective is to evaluate whether each candidate material system preserves a safe clearance boundary above the cranial headform under its unique quasi-dynamic force vector.

Assuming an initial designed unladen gap height of $d_{initial}$ = 30.0 mm between the helmet apex mid-surface and the skull crown, the residual clearance distance (d_{res}) is extracted using the relationship defined in (22). Table 5 summarizes the maximum vertical downward deflections ($\delta_{\max}$), the resulting residual clearance spaces, and the margin of safety values relative to the mandatory bottoming-out failure threshold ($d_{\min}$ = 15.0 mm).

Table 5. Finite Element Clearance Verification and Bottoming-Out Margin Summary ($d_{initial}$ = 30.0 mm, $d_{\min}$ = 15.0 mm)

Material System	HDPE (Base line)	Glass / Epoxy	Carbon / Epoxy	Kevlar / Epoxy
Thikness t[mm]	4.0	2.2	1.5	1.8
Applied Load $F_{e,d}$ [N]	4258.2	17408.0	24572.9	21094.7
Max Deflection $\delta_{\max}$ [mm]	14.80	8.11	5.14	6.69
Residulal Clearance d_{res} [mm]	15.20	21.89	24.86	23.31
Preliminary Structural Assessment	Marginal structural retention	Promising structural retention	High clearance retention	Promising structural retention

4. CONCLUSION

This study presented a multi-scale finite element framework to evaluate the feasibility of replacing conventional High-Density Polyethylene (HDPE) shells in industrial safety headgear with 3D randomly oriented fibre-reinforced composites. Analytical micromechanics bounds and numerical Representative Volume Element (RVE) homogenization confirmed that Glass/Epoxy, Carbon/Epoxy, and Kevlar/Epoxy systems deliver significantly higher specific stiffness and strength compared to HDPE, enabling substantial reductions in shell thickness and overall helmet weight.

The energy-balance derivation provided a conservative mapping of dynamic impact events into equivalent static forces, ensuring compliance with ANSI and EN safety standards. While the static approximation highlighted the stiffness–force paradox, the incorporation of dynamic amplification factors and nonlinear

considerations offers a pathway toward realistic simu–lation fidelity.

Overall, the results demonstrate that discontinuous fibre composites represent promising candidate mate–rials for lightweight industrial helmet shell concepts within a preliminary comparative engineering frame–work. However, challenges remain in addressing matrix brittleness, manufacturing-induced orientation biases, and cost-effectiveness. Future work should focus on dynamic drop tower validation, strain-rate characteri–zation, and full-scale prototype testing to bridge the gap between computational predictions and industrial imp–lementation.

The presented methodology should be interpreted as a preliminary engineering screening framework rather than a full dynamic certification model, with future work focused on explicit transient impact validation and experimental verification.

The proposed framework provides a practical engineering tool for preliminary material screening and helmet-shell redesign. By linking microstructural mate–rial properties with shell-level structural response, the methodology enables designers to quantify the potential benefits of alternative composite materials in terms of specific stiffness, shell-thickness reduction, mass redu–ction, and preservation of protective clearance. In this way, the study supports the development of lighter and structurally more efficient industrial safety helmets while providing a rational basis for early-stage material se–lection and design optimization. Nevertheless, the pro–posed approach remains a preliminary engineering scre–ening framework, and final certification-level assessment requires explicit transient impact simulations, strain-rate-dependent material characterization, and experimental validation through full-scale prototype testing.

ACKNOWLEDGMENTS

The authors would like to express their sincere gratitude to Prof. Dr. Mirko Dinulović for his valuable support and assistance, as well as for providing access to the Aeroelasticity Laboratory of the Department of Aeronautics, University of Belgrade Faculty of Mechanical Engineering, where the numerical computations and finite element analyses presented in this study were carried out.

REFERENCES

[1] Dinulović, M., Rašuo, B., Krstić, B., Bojanić, A.: 3D random fiber composites as a repair material for damaged honeycomb cores, FME Transactions, Vol. 41, No. 4, pp. 325-332, 2013.

[2] Rebhi, L., Dinulović, M., Dunjić, M., Grbović, A., Krstić, B. Calculation of the Effective Shear Modulus of Composite Sandwich Panels. FME Transactions, Vol. 45, No. 4, 2017.

[3] Dinulović, M., Rašuo, B., Krstić, B.: 3D Random Fiber Composites Application for the Honeycomb Core Repair, in: *Proceedings of the ICCE-21 - The 21st Annual International Conference on Composites/ Nano Engineering*, 21-27.7.2013, Tenerife, Spain, CD Rom, pp. 1-2.

[4] Goldsmith, W.: Impact: The Theory and Physical Behaviour of Colliding Solids, London: Edward Arnold, 1960.

[5] Johnson, K. L.: Contact Mechanics, Cambridge: Cambridge University Press, 1985.

[6] Kanit, T., Forest, S., Galliet, I., Mounoury, V. and Jeulin, D.: Determination of the size of the repre-sentative volume element for random composites: statistical and numerical approach, Int. J. Solids and Structures, Vol. 40, No. 13-14, pp. 3647-3679, 2003.

[7] Geers, M.G.D., Kouznetsova, V.G. and Brekelmans, W.A.M.: Multi-scale computational homogeniza-tion: trends and challenges, J. Comp. Appl. Math., Vol. 234, No. 7, pp. 2175-2182, 2010.

[8] Schneider, M.: Representative volume elements for matrix-inclusion composites - a computational study on sampling strategies and boundary effects, J. Mech. Phys. of Solids, Vol. 158, 104652, 2022.

[9] Hill, R.: Elastic properties of reinforced solids: some theoretical principles, J. Mech. Phys. of Solids, Vol. 11, No. 5, pp. 357-372, 1963.

[10] Miehe, C., Schröder, J. and Schotte, J.: Computa-tional homogenization analysis in finite plasticity, Comp. Meth. Appl. Mech. Eng., Vol. 171, No. 3-4, pp. 387-418, 1999.

[11] Voigt, W.: Ueber die Beziehung zwischen den beiden Elasticitäts constantan isotroper Körper, Annalen der Physik, Vol. 274, No. 12, pp. 573-587, 1889.

[12] Reuss, A.: Berechnung der Fließgrenze von Mi-schkristallen auf Grund der Plastizitäts bedingung für Einkristalle, Zeitschrift für Angewandte Mathematik und Mechanik, Vol. 9, Vo. 1, pp. 49-58, 1929.

[13] Hashin Z. and Shtrikman, S.: A variational approach to the theory of the elastic behaviour of multiphase materials, J. Mech. Phys. of Solids, Vol. 11, No. 2, pp. 127-140, 1963.

[14] Halpin, J.C. and Tsai, S.W.: Effects of environ-mental factors on composite materials, AFML-TR-67-423, Air Force Materials Laboratory, Wright-Patterson Air Force Base, 1969.

[15] Gibson, R.F.: Principles of Composite Material Mechanics, 4th ed. Boca Raton, FL: CRC Press, 2016.

[16] Advani, S.G. and Tucker III, C.L.: The use of tensors to describe and predict fiber orientation in short fiber composites, J. Rheology, Vol. 31, No. 8, pp. 751--784, 1987.

[17] Abrate, S.: The mechanics of short-fiber-reinforced composites: a review, Comp. Eng., Vol. 4, No. 7, pp. 731--772, 1994.

[18] Mallick, P.K.: Fiber-Reinforced Composites: Materials, Manufacturing, and Design, 3rd ed. Boca Raton, FL: CRC Press, 2007.

[19] Bottlang, M., Rouhier, A., Tsai, B., Madey, J., McIntosh, S. and Scher, S.: Effect of helmet design on impact performance of industrial safety helmets, Annals of Work Exp. and Health, Vol. 66, No. 6, pp. 755--766, 2022.

[20] Wu, J. Z., Pan, J., Welcome, J.P., Dong, R.G. and McDowell, T.W.: Testing the shock protection performance of Type I industrial helmets, Int. J. Ind. Ergonomics, Vol. 102, 103601, 2024.

[21] ANSI/ISEA: ANSI/ISEA Z89.1-2014 (R2019), American National Standard for Industrial Head Protection}. Arlington, VA: International Safety Equipment Association, 2019.

[22] CEN: EN 397:2025: Industrial Protective Helmets. Brussels: European Committee for Standardization, 2025.

NOMENCLATURE

C_{eff}	effective macroscopic stiffness matrix
D	flexural stiffness per unit width
d	fiber diameter
$d_{initial}$	initial clearance between helmet shell and headform
d_{res}	residual clearance between helmet shell and headform
d_{min}	minimum allowable residual clearance
E	Young's modulus
E_f	fiber Young's modulus
E_m	matrix Young's modulus
E_{eff}	effective Young's modulus
E_{Voigt}	Voigt upper-bound effective modulus
E_{Reuss}	Reuss lower-bound effective modulus
F_e	equivalent static force
$F_{e,dynamic}$	dynamic-equivalent static target force
FI	failure index
G	shear modulus
G_f	fiber shear modulus
G_m	matrix shear modulus
G_{eff}	effective shear modulus
G_{HS}^{upper}	Hashin-Shtrikman upper bound for shear modulus
h	impactor drop height
K	global structural stiffness; bulk modulus when used in micromechanics context
K_f	fiber bulk modulus
K_m	matrix bulk modulus
K_{eff}	effective bulk modulus
K_{HS}^{upper}	Hashin-Shtrikman upper bound for bulk modulus
L	fiber length
L_i	RVE periodicity vector
m	impactor mass
t	shell thickness
t_{comp}	composite shell thickness
t_{HDPE}	reference HDPE shell thickness
U_k	kinetic energy of impactor
U_s	elastic strain energy
u, v, w	displacement components
u_0, v_0, w_0	mid-surface translational displacements
V_0	impact velocity immediately before shell contact
V_f	fiber volume fraction
z	through-thickness coordinate measured from shell mid-surface
E/ρ	specific stiffness

Greek symbols

α	fiber finite aspect ratio, α = L/d
α_d	dynamic multiplier
δ	variation operator / virtual quantity
δ_{max}	maximum structural deflection
$\delta\varepsilon$	virtual strain tensor
δu	virtual displacement vector
ε	strain tensor / macroscopic strain tensor
ε_m	membrane strain tensor
γ_s	transverse shear strain tensor
κ	curvature tensor
η	Halpin-Tsai parameter
η_{mass}	mass-saving efficiency
θ	fiber orientation angle
θ_x, θ_y	shell-section rotations
ν_{eff}	effective Poisson's ratio
ρ	density
ρ_{eff}	effective density
ρ_{comp}	composite density
ρ_{HDPE}	HDPE density
σ	stress tensor
σ_{vM}	equivalent von Mises stress
σ_{all}	allowable stress / strength
ξ	Halpin-Tsai geometry parameter
Ω_{shell}	shell structural domain

Superscripts

f	fiber
m	matrix
eff	effective / homogenized property
$comp$	composite
$HDPE$	HDPE reference material
HS	Hashin-Shtrikman
max	maximum value
min	minimum value

initial	initial value
res	residual value
dynamic	dynamic-equivalent quantity
upper	upper bound
lower	lower bound

Abbreviations (

BMC	Bulk Molding Compound
FEA	Finite Element Analysis
HDPE	High-Density Polyethylene
HS	Hashin-Shtrikman
MPC	Multi-Point Constraint
PBC	Periodic Boundary Conditions
RVE	Representative Volume Element
SMC	Sheet Molding Compound

УПОРЕДНА АНАЛИЗА КОМПОЗИТНИХ МАТЕРИЈАЛА СА ТРОДИМЕНЗИОНАЛНО ОРЈЕНТИСАНИМ ВЛАКНИМА ЗА ИЗРАДУ ИНДУСТРОЈСКИХ ЗАШТИТНИХ ШЛЕМОВА

Н. Б. Ћурчић, М.Р. Трнинић, Д.Д. Гардашевић, Н. Д. Милошевић

Овај рад истражује замену конвенционалних шко–љки заштитних индустријских шлемова, израђених од полиетилена високе густине (HDPE) са ком–позитним материјалима са тродимензионално ори–јентисаним влакнима (стакло/епокси, карбон/епокси и кевлар/епокси). Развијен је модел заснован на методи коначних елемената који повезује хомоге–низацију репрезентативног запреминског елемента (RVE) на микро-нивоу са симулацијама танких љуски на макро-нивоу. Аналитичке границе микро–механике упоређене су са резултатима RVE високе прецизности како би се проценила ефективна изотропна еластична својства.

Хомогенизована и специфична крутост компо–зитних система показују значајна побољшања у односу на HDPE, омогућавајући знатно смањење дебљине и масе шкољке, заштитног индустријског шлема, уз задржавање заштитно померања мате–ријала. Композити на бази карбона и кевлара са епоксидном смолом показали су највишу спе–цифичну крутост и перформансе задржавања заш–титног померања материјала, међу испитиваним материјалима. Ипак, крутост матрице, одступања у оријентацији влакана изазвана производњом и трошкови остају важни фактори за разматрање.

Стога, дисконтинуирани влакнасти композити нуде обећавајући пут ка лакшим и ергономичнијим концептима шкољке заштитног индустријског шле–ма, при чему су потребна даља истраживања у обла–сти динамичке провере и испитивања прототипова